Experiments and analysis of combined diffraction and self-diffraction effects in a nematic-liquid-crystal cell

S. J. Elston, D. J. Webb,* and L. Solymar
Holography Group, Department of Engineering Science, University of Oxford, Parks Road, Oxford, OX1 3PJ, England
(Received 3 August 1992)

The potential for nonlinear optical processes in nematic-liquid-crystal cells is great due to the large phase changes resulting from reorientation of the nematic-liquid-crystal director. Here the combination of diffraction and self-diffraction effects are studied simultaneously by the use of a pair of focused laser beams which are coincident on a homeotropically aligned liquid-crystal cell. The result is a complicated diffraction pattern in the far field. This is analyzed in terms of the continuum theory for liquid crystals, using a one-elastic-constant approximation to solve the reorientation profile. Very good comparison between theory and experiment is obtained. An interesting transient grating, existing due to the viscosity of the liquid-crystal material, is observed in theory and practice for large cell-tilt angles.

PACS number(s): 61.30.Gd, 42.40.Lx

I. INTRODUCTION

Nonlinear optical effects in liquid crystals have now been investigated for over a decade. The main reason is that significant effects can be found in relatively thin samples with laser intensities as small as 100 W/cm^2. For example, a 100-μm-thick layer of material can provide tens of π phase changes in the phase of transmitted light. The origin of this effect may be thermal (relying on the temperature dependences of the indices of refraction, which are particularly large in the vicinity of the phase-transition temperature) or due to the reorientation of the liquid-crystal molecules. In the latter case the full anisotropy of the dielectric constant may be utilized. The relative permittivity at optical frequencies might vary by as much as 0.5 for a reasonable range of input intensities.

In order to have nonlinear effects the light intensity needs to vary. This may occur when the intensity varies within a single beam. For a Gaussian input beam, for example, it has been known for a long time that it may cause the appearance of a spectacular ring pattern in the far field [1,2]. Intensity variation may also be produced by two coherent plane waves incident at a certain interbeam angle. They give rise to an interference pattern that leads to a periodic variation of the index of refraction which, in turn, will diffract the incident beams. If the interbeam angle is small enough the dominant mechanism is Raman-Nath diffraction (in contrast to Bragg diffraction), producing multiple output beams [3]. Self-diffraction and Raman-Nath diffraction effects may also be present simultaneously if the interfering beams have Gaussian intensity distributions as shown by Jun and Eichler [4] in silicon, and by Venables and Tunnicliffe [5] in liquid crystals utilizing thermal gratings. More detailed experiments on the combined effect were recently done by Webb, Elston, and Solymar [6] relying on reorientation gratings.

There was no attempt in Refs. [4] and [5] to describe the effect theoretically. In the paper by Webb, Elston, and Solymar it was argued that the joint effect of self-diffraction and Raman-Nath diffraction may be taken into account simply by considering the contribution of each effect to the phase of the output electric field of the optical beams. One may expect a Gaussian phase distribution due to the Gaussian intensity distribution of the input beams and a periodic phase distribution due to the effect of interference between the two beams. Such an approach did indeed lead to good qualitative agreement between theory and experiment by making inspired guesses about the time variation of the relative magnitudes of the Gaussian and of the periodic parts. However, the method did not permit to relate in any way the measured diffraction pattern to the parameters of the liquid-crystal cell.

The aim of the present paper is to investigate this combined effect in more detail experimentally and with more rigor theoretically. We shall solve the time- and space-varying macroscopic equations of the reorientation of the director of the liquid-crystal molecule.

In Sec. II we shall discuss the theory and the method of numerical solution. The experimental set up will be described in Sec. III together with the results of the measurements. In Sec. IV the theoretical and experimental diffraction patterns will be compared, and conclusions will be drawn in Sec. V.

II. THEORY

The continuum theory of nematic liquid crystals is based on the minimization of the free energy of the material, under distortions induced in the director profile [7]. There are three elastic constants associated with distortion, termed splay, and twist and bend constants [8]. For most materials these are around 10^{-12} N, and to a first order can be approximated by one constant. Minimization of the resulting free-energy equation then allows the derivation of a differential equation relating the spatial variation of the director to the force on the director due to some external electric field. If it is further assumed that the curvature of the reorientation profile is

small and that the time variation may be described using a single viscosity constant, our starting equation may be written as [3,9]

$$K\nabla^2\theta+\tfrac{1}{2}\Delta\epsilon\epsilon_0E^2\sin2(\theta-\beta)=\eta\frac{\partial\theta}{\partial t}\ , \tag{1}$$

where β is the tilt of the laser field from the relaxed director direction, K is the elastic constant, θ is the reorientation angle, $\Delta\epsilon$ is the dielectric anisotropy, ϵ_0 is the free space permittivity, E is an electric field, ∇ is the spatial differential operator, t is time, and η is the viscosity coefficient. This approach has previously been used to successfully model both self-diffraction effects [10,11] and diffraction from light-induced gratings [3] in nematic liquid crystals using analytical and numerical techniques. For mathematical convenience we normalize to d, the thickness of the cell being used, and write

$$\nabla^2\theta+\Omega\sin2(\theta-\beta)=\eta'\frac{\partial\theta}{\partial t}\ , \tag{2}$$

where

$$\Omega=\frac{\Delta\epsilon\epsilon_0E^2d^2}{2K}\ ,\quad \eta'=\frac{\eta d^2}{K}\ .$$

We wish to solve Eq. (2) for the experimental arrangement shown in Fig. 1. There are two Gaussian beams of circular cross section incident at an interbeam angle of ϕ upon a homeotropically oriented liquid-crystal cell which is tilted by the angle β_{ext} relative to the plane of the incident beams. The electric-field polarization is assumed to be perpendicular to the plane of incidence and the spatial variation of E^2 is taken in the form

$$E^2=4E_0^2\cos^2\frac{K_gy}{2}\exp\left[-\frac{2r^2}{w^2}\right]\ , \tag{3}$$

where E_0 is the peak field, the same for both beams, K_g is the magnitude of the grating vector ($K_g=2\pi\sin\phi/\lambda$), r is the radial dimension, and w is the $1/e$ ($1/e^2$ in intensity) beam radius. We may therefore write

$$\Omega=\Omega_0\cos^2\frac{K_gy}{2}\exp\left[-\frac{2(x^2+y^2)}{w^2}\right]\ . \tag{4}$$

Note that by writing the electric field in the form of Eq. (4) some approximations have been made. It was neglected that the two beams propagate in slightly different directions and consequently their cross sections will be slightly elliptical and they do not exactly coincide. The essential features of the interaction are of course retained in the sense that K_g describes the spatial variation due to the interference of the two beams and the Gaussian functions describe the spatial variation of the individual beams.

Equation (2) may now be solved in principle but as there is no chance of obtaining an analytical solution we used the following numerical method. The cell is split into a three-dimensional grid of points and $\nabla^2\theta$ and $\Omega\sin2(\theta-\beta)$ are calculated at each point. This will determine the right-hand side of Eq. (2), i.e., we obtain the gradient $\partial\theta/\partial t$ from which a new value of θ can be calculated a small time interval later. Repeating this process allows the solution to be found, the steady-state being reached when $\partial\theta/\partial t\Longrightarrow0$. The initial condition is that the reorientation angle is zero everywhere. The boundary conditions are chosen so that at all times the reorientation angle is kept zero at the surfaces $z=0$ and d (due to the homeotropic orientation) and at a distance two beam radii away from the center of the beam in the radial direction. Stability of the solution is ensured by using sufficiently small time steps.

Having determined the reorientation profile we need to determine the variation of the optical field. We shall rely on the well-known optical-path method, according to which the propagation direction of the optical wave remains unchanged, but its phase changes as it traverses the cell. Since we know the spatial distribution of the reorientation angle we know also the spatial distribution of both indices of refraction, which then allows us to find the phase of the electric field at the output surface $z=d$. The amplitude of the field is assumed to be unchanged. We may then take a two-dimensional Fourier transform of the output electric field to obtain the far-field diffraction pattern.

Calculation of the far-field pattern in this way ignores the diffraction effects that may take place within the liquid-crystal cell itself. Such effects could be significant for the large phase changes involved in the cell. However, if the cell is thin enough their influence on the diffraction pattern is likely to be small. This appears to be the case under the conditions investigated in the present paper as implied by the good agreement between theory and experiment.

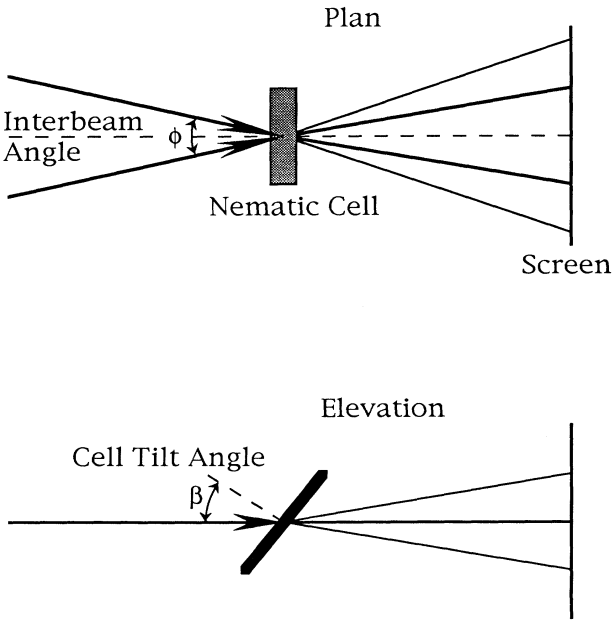

FIG. 1. Experimental arrangement. The two incident s-polarized Ar^+-laser beams (at 514.5 nm) with spot size of 200 μm intersect at an angle of 25 mrad on a cell tilted by an angle of β_{ext}. The cell is a 100-μm thick, homeotropically aligned 5CB. The resulting far-field diffraction pattern is observed on the screen and recorded on a VTR.

III. EXPERIMENTS

The experimental arrangement is identical with that of Webb, Elston, and Solymar [6]. An argon-ion-laser beam at 514.5 nm is split into two equal-intensity beams that are then focused together onto a homeotropically aligned nematic-liquid-crystal cell containing the material 4-*m*-pentyl-4′-cyanobiphenyl (5CB), as shown in Fig. 1. The two incident beams are carefully aligned to cross in the cell, with a spot size of 200 μm. The interbeam angle can be varied, but the results and theory presented here are all for an interbeam angle of 25 mrad. This shows well the features of both Raman-Nath and self-diffraction effects. The resulting far-field diffraction pattern is observed on a screen behind the cell and the temporal development of the pattern after opening the laser shutter is

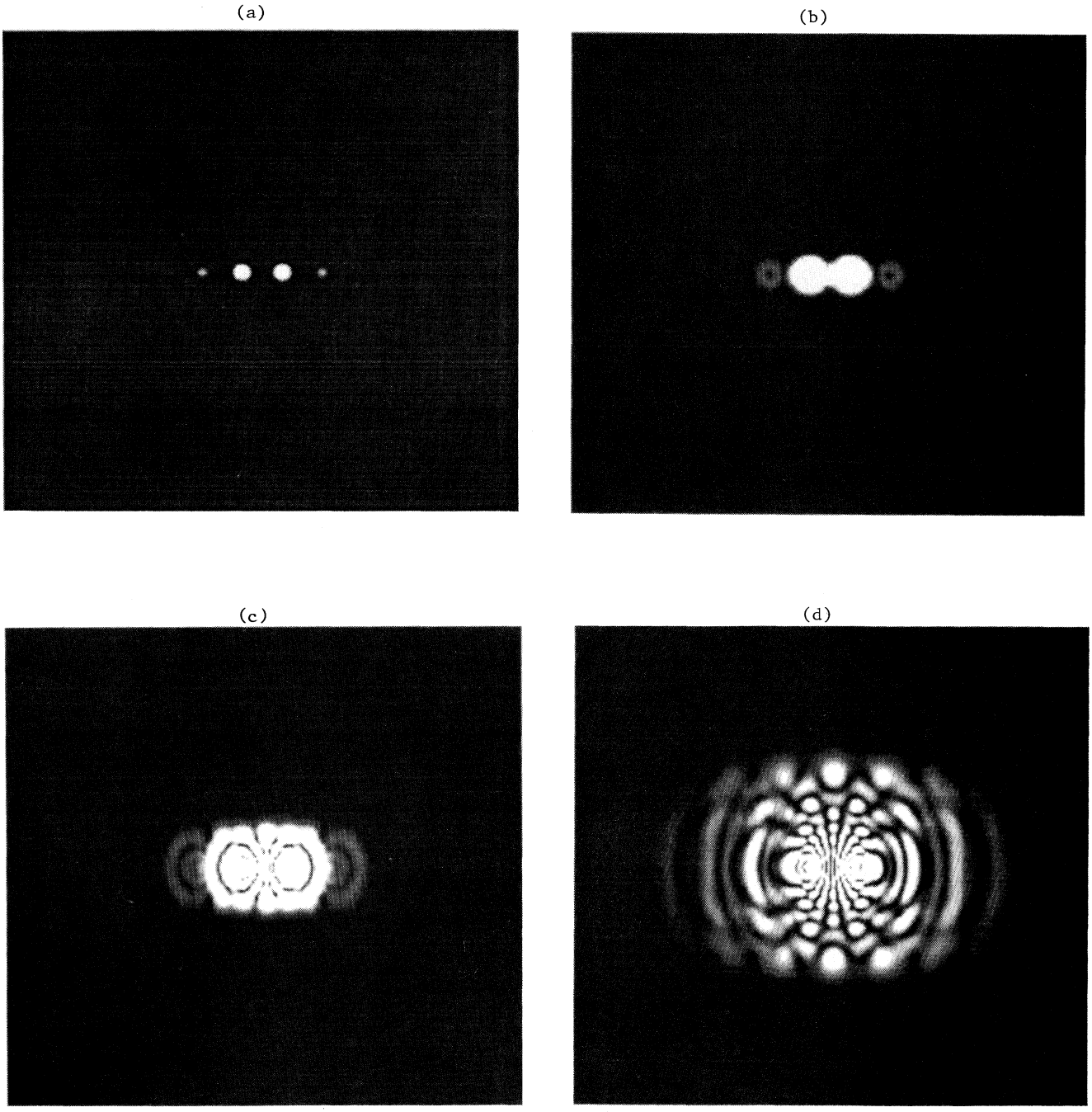

FIG. 2. Theoretical development of the diffraction pattern in the fair field for a cell-tilt angle of $\beta_{ext}=5°$. The parameters were fixed at $\Omega_0=25$ and $\eta/K=2\times10^{10}$ m^{-2} s, as discussed in the text. The times shown are (a) 2 s; (b) 10 s; (c) 20 s; (d) 40 s; (e) 200 s, the last having reached steady state.

(e)

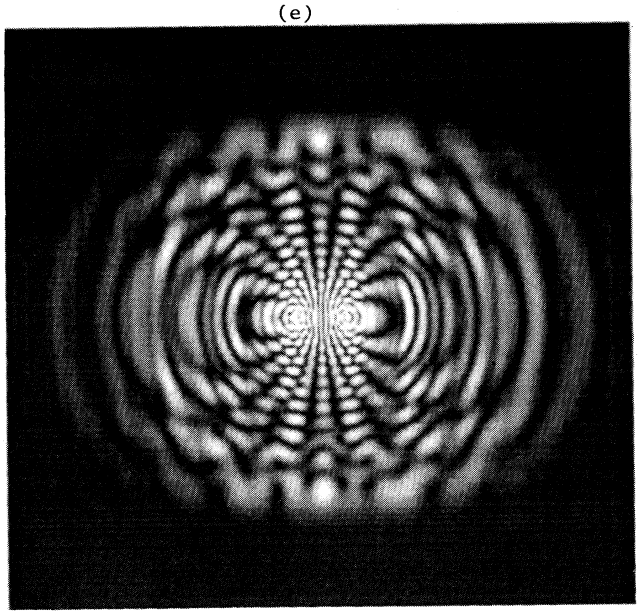

FIG. 2. (*Continued*).

recorded on a video tape recorder (VTR). This allows the slow time development of the effects to be monitored and carefully examined, although the rapid Raman-Nath development for large cell-tilt angles is on the edge of the time resolution of this technique. We have also verified that by blocking one of the beams our complicated pattern reduces to the well-known ring pattern [1,2]. Taking data in the manner described it is observed that a lot of scatter takes place in the cell. This is characteristic of thick layers of nematic material—in fact the cell looks slightly milky under white light illumination.

For shallow cell-tilt angles (β_{ext} about 5°) the buildup of the diffraction pattern is quite slow, taking several seconds to show weak Raman-Nath effects. These effects do not persist and are soon overtaken by the self-diffraction effects which result in rings around the two laser spots and the Raman-Nath spots [6]. The pattern becomes more complicated as the rings from the laser spots and Raman-Nath spots begin to overlap. The time period needed to reach steady state is about 2 min. This steady state shows a complicated two-dimensional array of fringes and fluctuation of light patterns in the far field. The fluctuation is due to the fluctuation of the director in the nematic cell.

For steeper cell-tilt angles (β_{ext} about 45°) the buildup of the diffraction pattern is much faster. This is because the initial torque on the director, proportional to $\sin 2(\theta-\beta)$, is much larger. Then the Raman-Nath effect develops in a few hundred milliseconds, and shows up to about eight Raman-Nath spots. These then break up into rings and develop as before. The patterns in this case are less well defined. The reasons for the differences are not clear, but may be due to the laser beam traveling through a thick layer of the nematic material and greater scattering taking place.

It is then these developments which we wish to model numerically, concentrating on the interesting features which occur initially, i.e., the development and breakup of the Raman-Nath-type diffraction. It is this which is most useful in nonlinear optical processes using liquid-crystal materials and which needs the theoretical development and modeling.

IV. RESULTS

We now show the theoretical results of the calculations and compare them with the diffraction seen experimentally. In order to make the theoretical calculations we need the values of a number of parameters. Some of these parameters follow from the experimental configuration. K_g can be calculated from the interbeam angle and the wavelength, the $1/e^2$ intensity spot of the focused beams can be measured, and the cell is known to be 100-μm thick. The values chosen correspondingly are

$$K_g = 3.05 \times 10^5 \text{ m}^{-1}, \quad w = 100\ \mu\text{m}, \quad d = 100\ \mu\text{m}.$$

There are still two parameters Ω_0 and η/K which need to be chosen. It is relatively easy to determine the value of Ω_0 by comparing the experimental and theoretical patterns for a single input beam. It is well known [1,2] that as a result of self-diffraction a number of rings appear and that the total number of rings is related to the total phase difference between the center and the edge of the beam. For a certain input power we obtained nine rings for $\beta_{\text{ext}} = 45°$, which from the theoretical modeling corresponded to $\Omega_0 = 25$, which is the value used in all our simulations. The value of η/K is chosen for best overall agreement with the data, for three values of β_{ext}, which gives $\eta/K = 2 \times 10^{10}$ m^{-2}s. This corresponds to that used by previous workers [12].

The resulting development of the theoretical diffraction pattern is shown in Figs. 2(a)–2(e) for times of 2, 10, 20, 40, and 200 s, respectively. The experimental diffraction patterns (computer reproductions of the relevant video frames) may be seen in Figs. 3(a)–3(e). In order to obtain the best agreement between the theoretical and experimental results it is necessary to depart from the time scale of the theoretical plots, meaning that the experimental and theoretical time scales do not coincide. The experimental plots are shown for times of 4, 20, 38, 50, and 200 s, respectively. The times for the development after initial illumination differ by a factor of 2, it taking 4 s to reach experimentally the situation theoretically predicted to exist at a time of 2 s. As time develops the error reduces, the theoretical situation at 40 s corresponding to the experiment at 50 s. While this could be improved by variation in the value of η/K, larger errors would then be introduced in the timing of results for larger cell-tilt (β_{ext}) angles. A potential error, and possible reason for the nonlinear scaling between theoretical and experimental times, may be in the use of the one-constant approximations for viscosity and elasticity.

The agreement between the patterns is, however, remarkably good. The initial Raman-Nath diffraction is reproduced, as is the development of the ring structure around the spots. This shows the initial development of a periodic reorientation profile in the liquid-crystal cell

which is followed by the development of an overall Gaussian profile leading to the appearance of self-diffraction rings. The experimental and theoretical diffraction patterns beyond this time [Figs. 2(d) and 2(e), and Figs. 3(d) and 3(e)] are still in good qualitative agreement although the precise spot distribution and number of spots is not perfectly reproduced in the theory. There are a number of reasons why this might be so. (i) The unperturbed Gaussian intensity distribution (i.e., before reorientation starts) is assumed not to vary with the z coordinate, whereas in reality it will change its shape and its phase front will have a quadratic component. (ii) The propagation direction of the optical beam is assumed to be unchanged, whereas in reality it will be influenced by the reorientation of the molecules. This will mostly affect the pattern in the steady state. (iii) As noted above, mod-

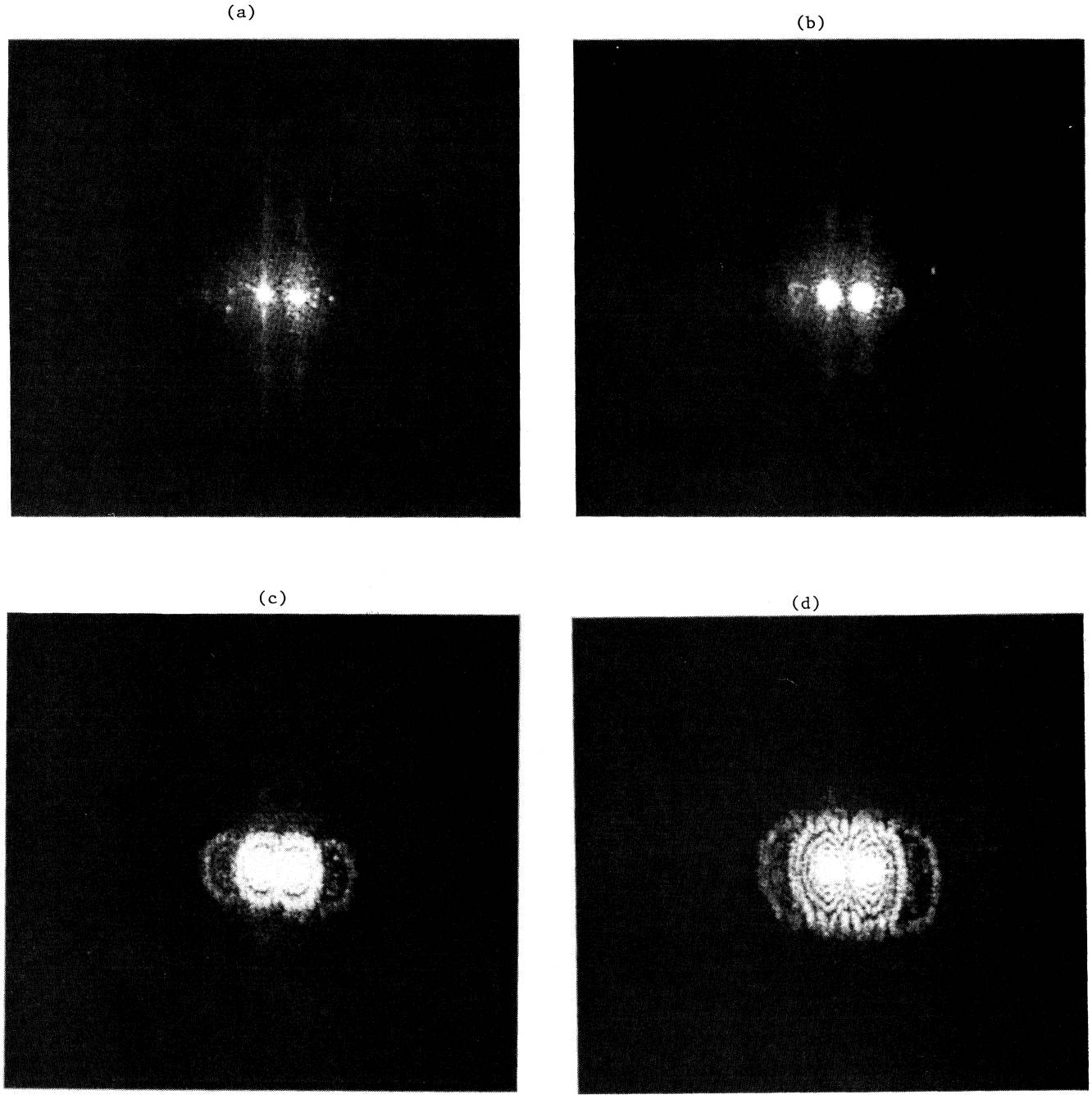

FIG. 3. Experimental results for the case theoretically modeled in Fig. 2, with images taken from a video sequence of the far-field diffraction-pattern development. The images are chosen to correspond with those shown in Fig. 2. The times are (a) 4 s; (b) 20 s; (c) 38 s; (d) 50 s; (e) 200 s.

(e)

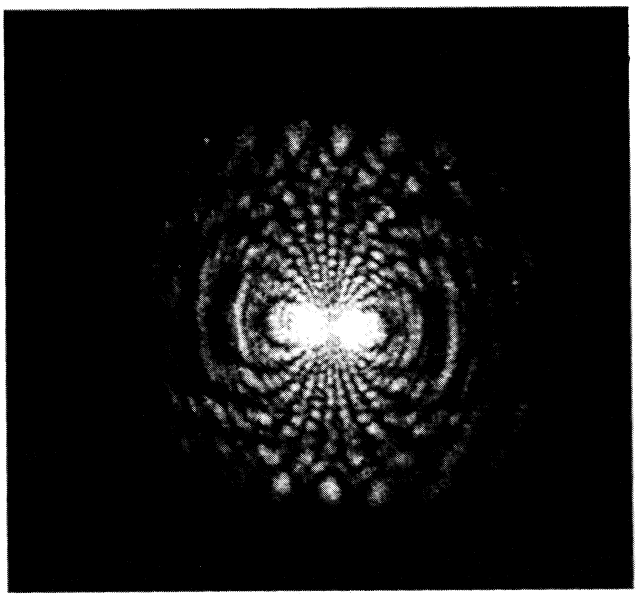

FIG. 3. (*Continued*).

eling with the one-elastic-constant and one-viscosity-constant approximations may be insufficient. (iv) Since we had three spatial variables plus one temporal variable it took considerable time (about 25 h of CPU time on our Sun workstation) to solve the differential equation for a single set of parameters, therefore, we may not have found the optimum value of η/K. We made no attempts either to change slightly the values of w and d that may not have been measured with sufficient accuracy. We believe, however, that within these constraints the modeling is good and shows the important features very well.

It is interesting to consider the form of the phase front of the transmitted light. This is shown for the saturation condition here in Fig. 4. This is as might be expected, and is as embodied in the previous intuitive model of Webb, Elston, and Solymar [6]. The broad form is an overall Gaussian, reflecting the reorientation caused by the Gaussian profile of the incident intersecting laser beams. A weak periodic oscillation in the phase front is also seen in this. The intensity of the incident laser power oscillates sinusoidally, between zero and the Gaussian level [see Eqs. (3) and (4)]; the resulting reorientation is, however, only weakly modulated due to the elastic interactions in the liquid-crystal material. Here the pitch of the interference pattern is about 20 μm, but

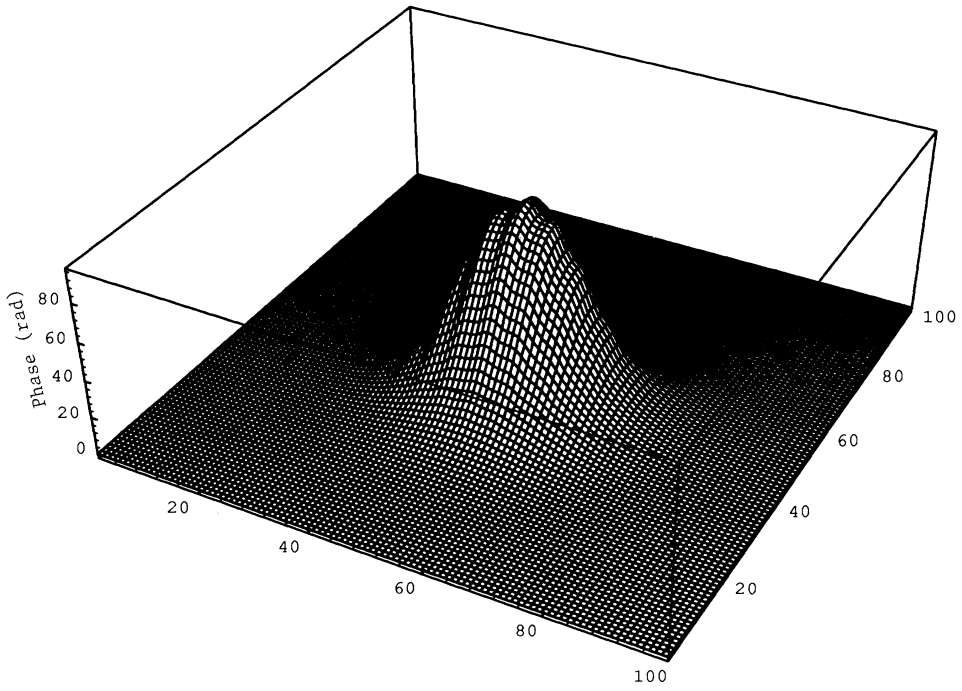

FIG. 4. Phase front of the transmitted light, calculated for the saturation condition at $\beta_{ext}=5°$. This shows the overall Gaussian form, reflecting the form of each incident beam, together with a weak periodic modulation due to the interference between the incident beams. The x and y scales are here in units of μm/4, as the 100-point grid is extended to 2 beam radii from the center.

the only force which could cause the director not to reorientate everywhere is the surface interaction, and as the cell is 100 μm thick this is only a weak effect. The result is a weak oscillation in the reorientation profile and the resulting weak oscillation in the resulting phase front of the transmitted light.

We can illustrate the buildup of the two parts (Gaussian and periodic) of the phase front by considering what happens in the center of the beams. We define the Gaussian part of the modulation as the difference between the phase at the edge and middle of the phase front, and the periodic part as being the amplitude of the modulation in the center of the phase front. Using this it is possible to plot a representation of the two parts of the phase front. For this cell-tilt angle ($\beta_{ext}=5°$) the time development of these two parts is shown in Figs. 5(a) and 5(b). It is seen that the periodic part and Gaussian part develop in roughly the same manner, as might be intuitively expected. The amplitudes are however vastly different, with the Gaussian part reaching a modulation of about 30π and the sinusoidal part reaching a modulation of only about π. In addition there are subtle differences for the start of the development; these will be commented on for the larger cell-tilt case.

We now show the initial development for the cases of tilts of $\beta_{ext}=20°$ and $\beta_{ext}=45°$. For both cases the long-time development and steady-state conditions are broadly similar to the $\beta_{ext}=5°$ case. All tilt angles show both in

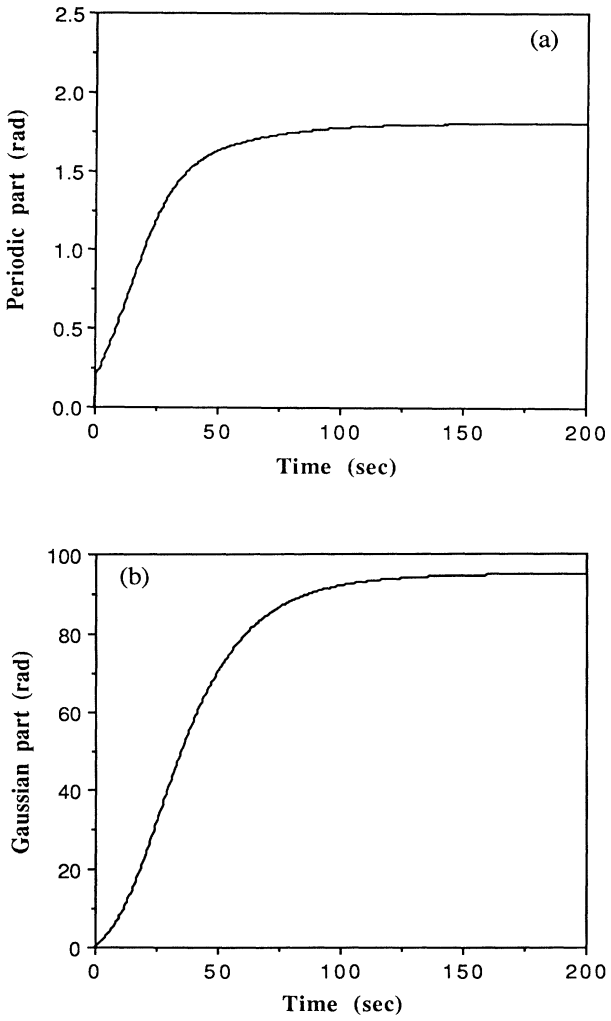

FIG. 5. Development of (a) the periodic part and (b) the Gaussian part of the transmitted phase front in the center of the beams, for $\beta_{ext}=5°$. The form of both is broadly the same, as may be expected, but the amplitudes are vastly different.

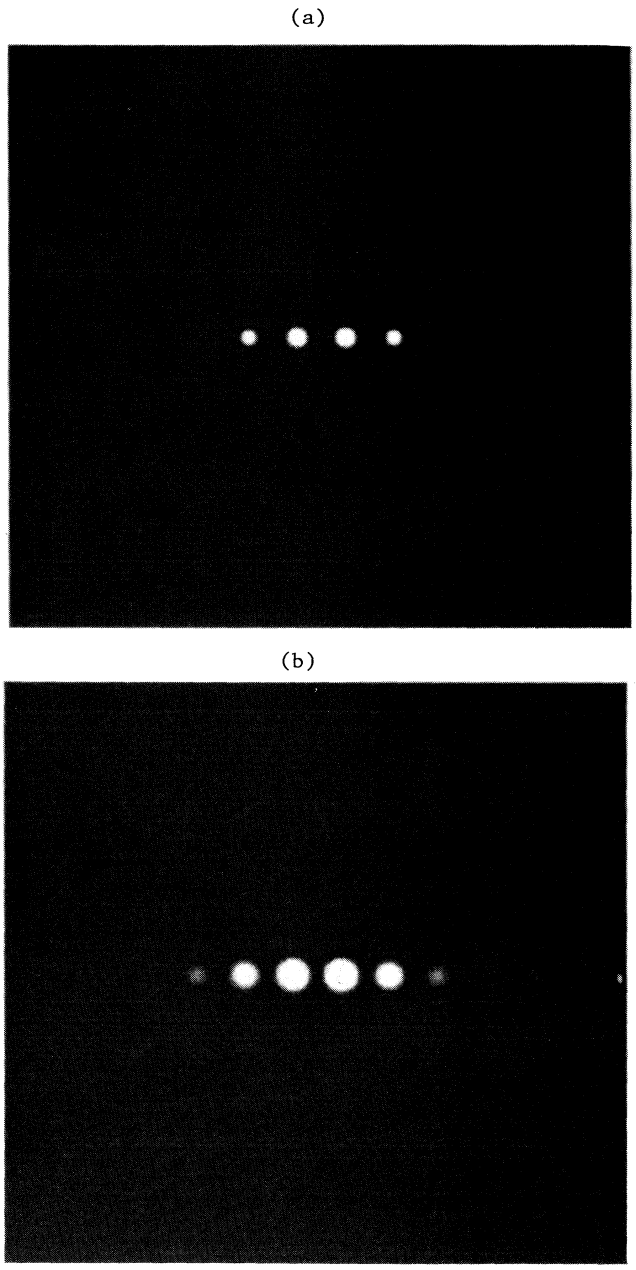

FIG. 6. Theoretical prediction of diffraction patterns for $\beta_{ext}=20°$. Only the initial development is shown for times of (a) 0.2 s and (b) 1 s, showing the prediction of up to six Raman-Nath spots in this case.

experiment and in theory the development of rings around the laser and Raman-Nath spots, which spread into one another and develop into a complicated pattern of the form shown in Figs. 2 and 3. The initial development does, however, speed up with increasing values of β_{ext}.

The theoretical predictions for the same set of parameters, but for $\beta_{ext}=20°$, are shown in Fig. 6. By $t=0.2$ s four spots appear [Fig. 6(a)] which grow into six spots by $t=1$ s, and one may observe the budding ring structure [Fig. 6(b)]. The corresponding experimental results are shown in Fig. 7 where the times are chosen as $t=0.25$ s

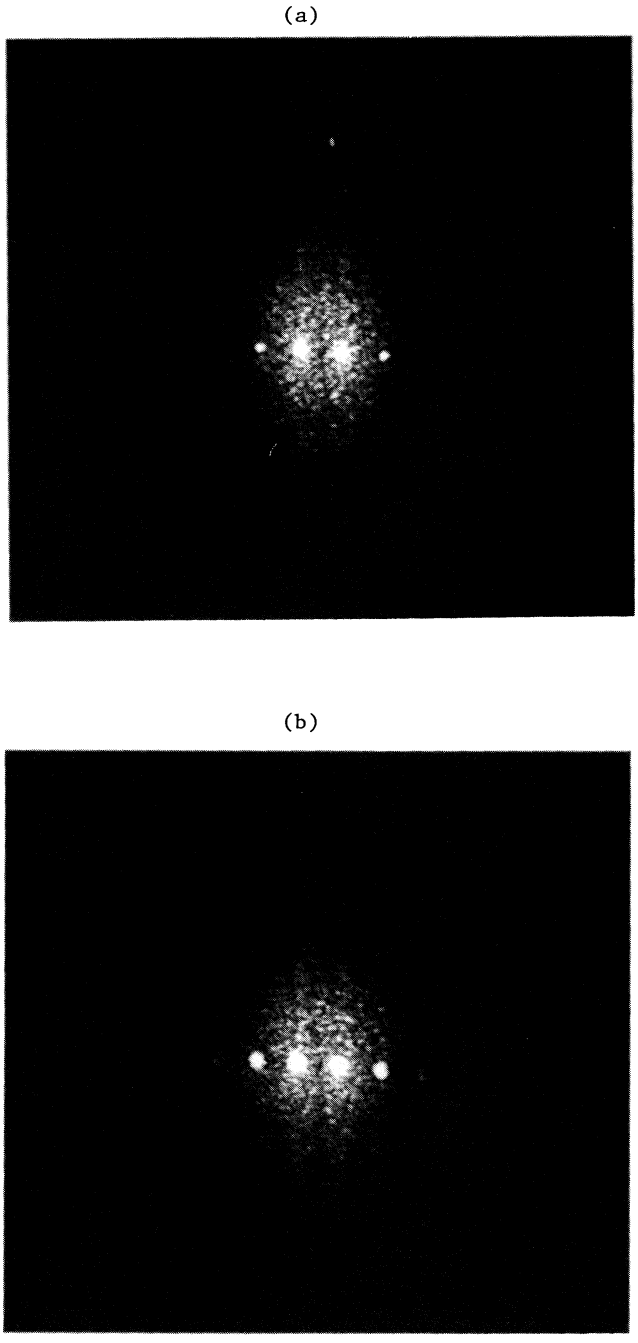

FIG. 7. Experimental results for $\beta_{ext}=20°$, corresponding to Fig. 6. the times are (a) 0.25 s and (b) 1 s, in this case in very good agreement with the theoretical predictions.

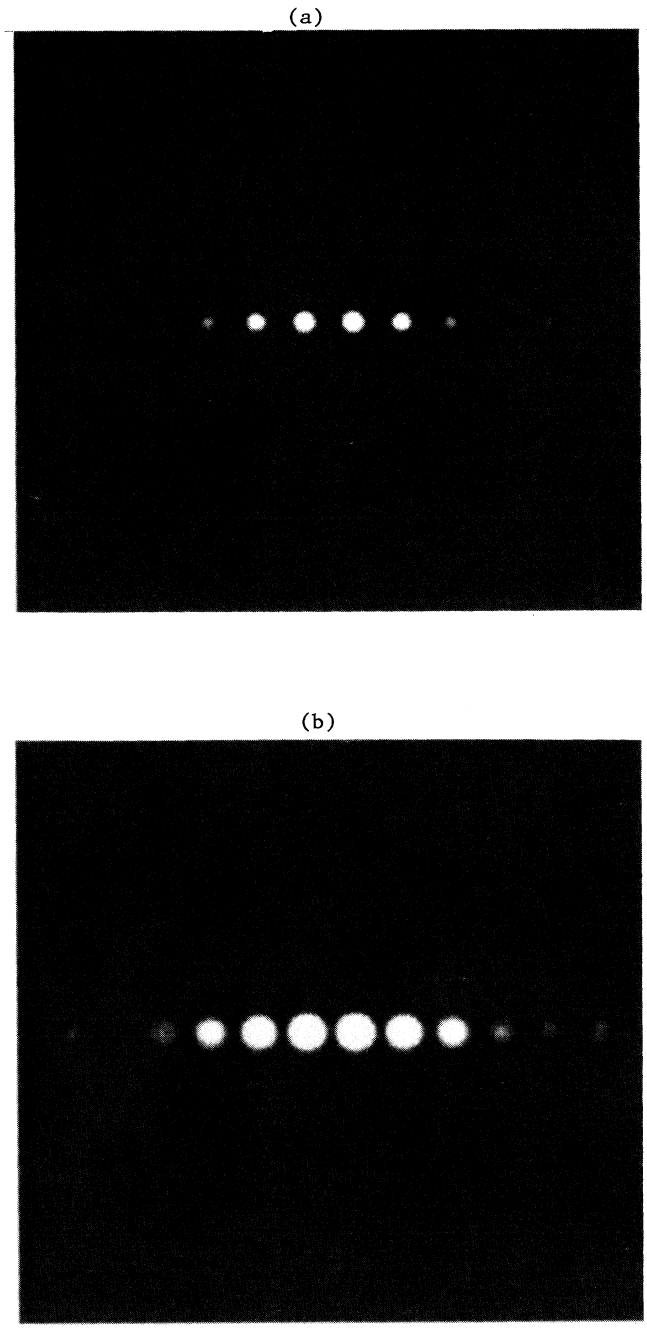

FIG. 8. Theoretical prediction for the initial development of the diffraction patterns for $\beta_{ext}=45°$. The times are (a) 0.08 s and (b) 0.4 s. In this case eight Raman-Nath spots are seen.

for Fig. 7(a) and $t=1$ s for Fig. 7(b). Unfortunately, there is a large amount of scattered light in the experimentally observed patterns but otherwise the agreement may be seen to be good.

Changing the external angle to $\beta_{ext}=45°$ the theory predicts six spots by $t=0.08$ s [Fig. 8(a)] and eight spots by $t=0.4$ s [Fig. 8(b)]. The experimental results for $t=0.12$ s [Fig. 9(a)] and $t=0.55$ s [Fig. 9(b)] again look similar.

One may conclude that for the higher angle the periodic part of the reorientation is stronger and it appears faster. We may again check this by determining, with the method outlined previously, the periodic and Gaussian contributions to the output phase angle of the transmitted beams. They are plotted in Figs. 10(a) and 10(b), respectively. The periodic part [Fig. 10(a)] varies more or less as expected. The new aspect is that, in contrast to that shown in Fig. 5(a), the periodic component of the phase initially overshoots and then declines for larger values of time. The two Gaussian contributions shown in Fig. 10(b) are very similar for the two angles.

It is interesting to consider the reason for the overshoot of the periodic part of the transmitted phase

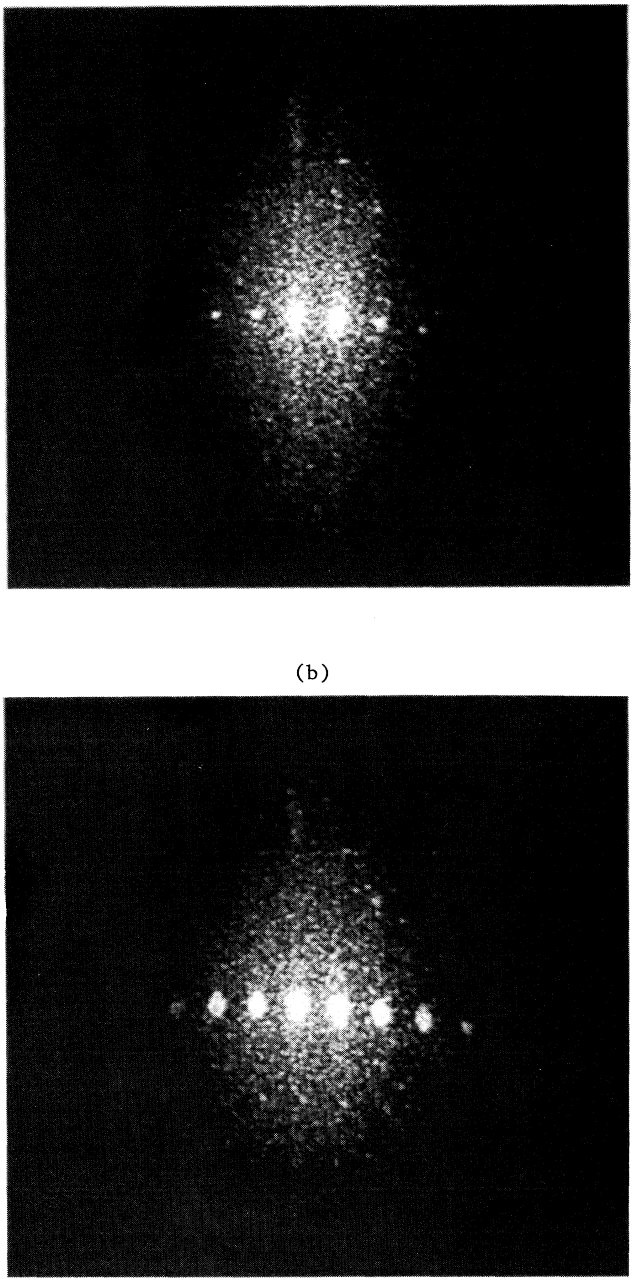

FIG. 9. Experimental results from the video for $\beta_{ext}=45°$, corresponding to the theory of Fig. 8. The times are (a) 0.12 s and (b) 0.55 s. The eight Raman-Nath spots are seen here in the experimental data as well, although there is a lot of optical scatter.

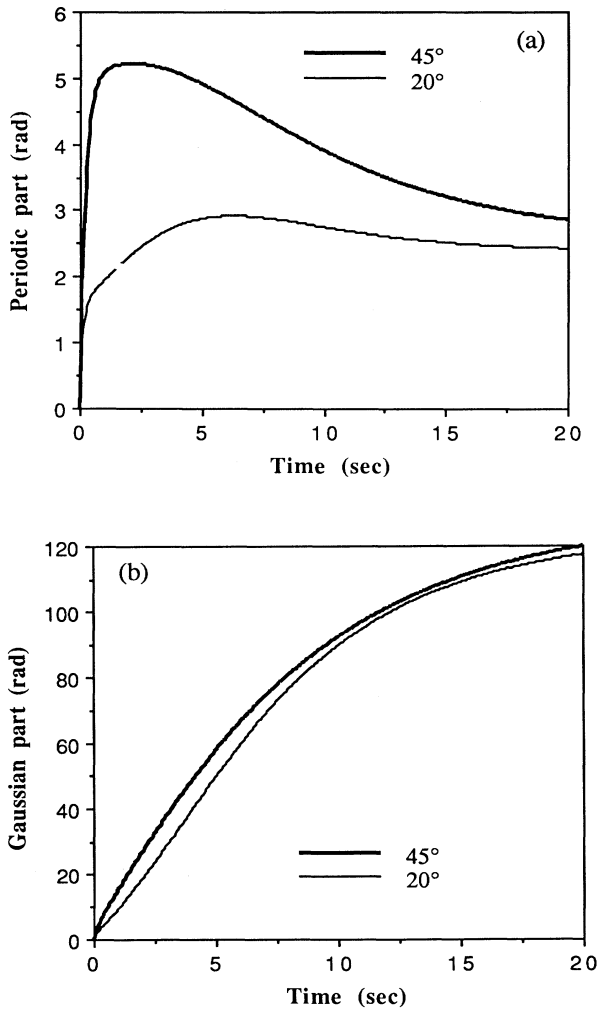

FIG. 10. Development of (a) the periodic part and (b) the Gaussian part of the transmitted phase front for the cases of $\beta_{ext}=20°$ and $\beta_{ext}=45°$. They are seen to be more rapid than in the $\beta_{ext}=5°$ case (Fig. 5), and a very interesting overshoot is seen in the periodic part for $\beta_{ext}=45°$. This occurs due to the viscosity of the liquid-crystal material, allowing the formation of a transient grating.

for the large cell-tilt angles. This effect is due to the viscosity of the nematic material. With large torques present (as we have for large cell tilts) the liquid-crystal director takes a relatively long time to respond to the liquid-crystal elastic forces in the nodes of the interference pattern between the incoming beams, due to the viscosity of the material. Thus a stronger transient grating is produced, which begins to decay after about 1 s. For a cell tilt of $\beta_{ext}=5°$, which has a much slower response, the effect remains as a knee in the periodic part of the phase front at a time of about 500 ms [see Fig. 5(b)].

V. CONCLUSIONS

We have compared directly the experimental results for diffraction from a nematic-liquid-crystal cell illuminated by a pair of incident laser beams with a theory based on the continuum mechanics of liquid-crystal materials. The comparison is seen to be good, with the predictions showing all of the main features of the experimental data. We have been able to model the form of the diffraction patterns, showing a combination of Raman-Nath and self-diffraction effects. The time dependence has been modeled by the use of a diffusion solution to the partial differential equation for the reorientation of the liquid-crystal director under an external laser field. Further, the effect of variation of the tilt angle of the cell on the observations are reproduced. Of particular interest is the variation in the Raman-Nath effects depending on the tilt of the cell and resulting torque on the director. The stronger (and faster) Raman-Nath diffraction seen for large tilts is important. It may be that this is the region that should be investigated with respect to the observation of multiwave (two, three, and four) interaction in liquid-crystal cells, and the search for useful gain mechanisms. The strongest Raman-Nath diffraction was seen (experimentally and theoretically) a few hundred milliseconds after illumination for cell tilt of about $\beta_{ext}=45°$—this time scale may similarly give good multiwave interactions. It would be interesting to investigate this more fully, and we aim to do so in the future.

ACKNOWLEDGMENTS

The authors acknowledge the Science and Engineering Research Council for support, and S.J.E. acknowledges the support of GEC and the Fellowship of Engineering.

*Now at Department of Physics, The University, Canterbury, Kent, CT2 7NR, England.

[1] N. F. Pilipetski, A. V. Sukhov, N. V. Tabiryan, and B. Ya. Zeldovich, Opt. Commun. **37**, 280 (1981).
[2] S. D. Durbin, S. M. Arakelian, and Y. R. Shen, Opt. Lett. **6**, 411 (1981).
[3] I. C. Khoo, IEEE J. Quantum Electron. **22**, 1268 (1986).
[4] C. Jun and H. J. Eichler, Appl. Phys. B **45**, 121 (1988).
[5] M. A. Venables and D. L. Tunnicliffe, J. Phys. D **22**, 225 (1989).
[6] D. J. Webb, S. J. Elston, and L. Solymar, Opt. Commun. **89**, 283 (1992).
[7] J. L. Ericksen, Mol. Cryst. Liq. Cryst. **7**, 153 (1969).
[8] F. M. Leslie, Adv. Liq. Cryst. **4**, 1 (1979).
[9] H. J. Eichler, R. MacDonald, and C. Dettmann, Mol. Cryst. Liq. Cryst. **174**, 153 (1989).
[10] I. C. Khoo, T. H. Liu, and P. Y. Yan, J. Opt. Soc. Am. B **4**, 115 (1987).
[11] L. B. Au, L. Solymar, C. Dettmann, H. J. Eichler, R. MacDonald, and J. Schwartz, Physica A **174**, 94 (1991).
[12] I. C. Khoo, R. G. Lindquist, R. R. Michael, R. J. Mansfield, and P. LoPresti, J. Appl. Phys. **69**, 3853 (1991).

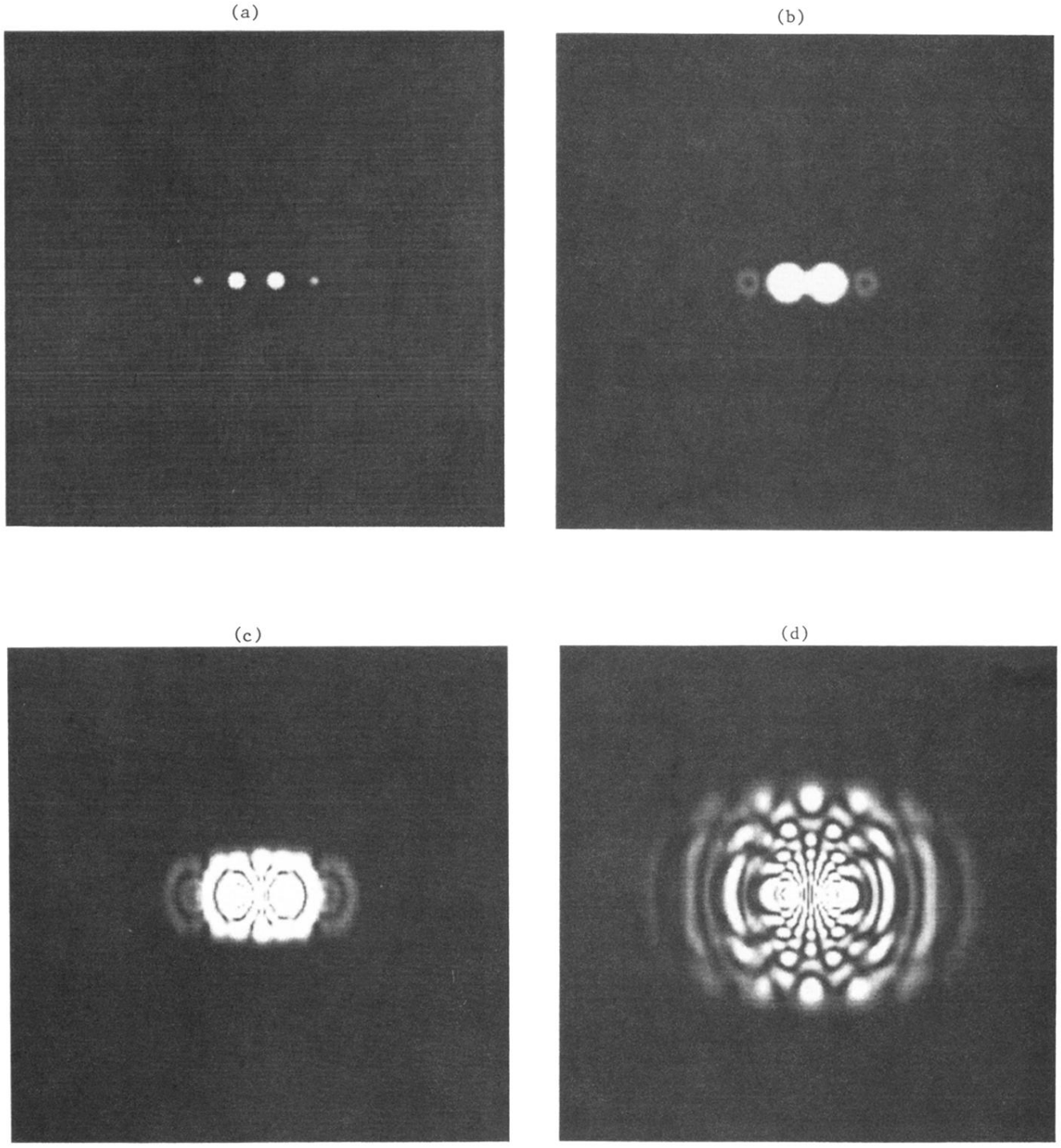

FIG. 2. Theoretical development of the diffraction pattern in the fair field for a cell-tilt angle of $\beta_{ext}=5°$. The parameters were fixed at $\Omega_0=25$ and $\eta/K=2\times10^{10}$ m^{-2} s, as discussed in the text. The times shown are (a) 2 s; (b) 10 s; (c) 20 s; (d) 40 s; (e) 200 s, the last having reached steady state.

(e)

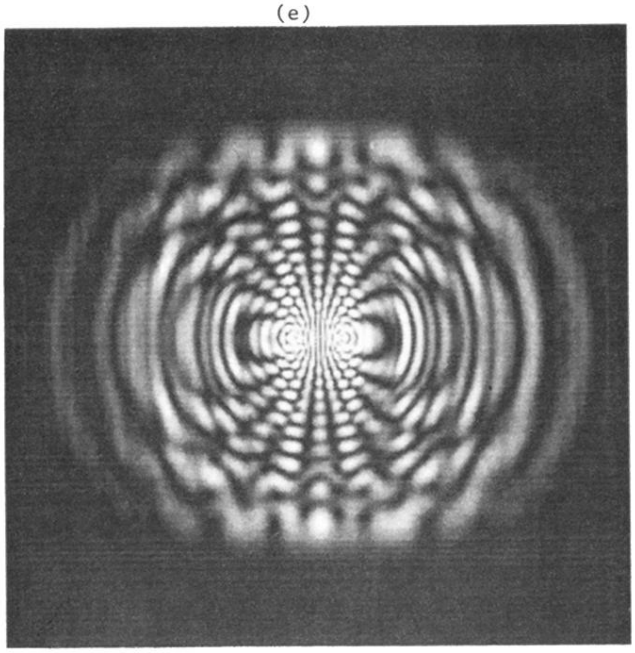

FIG. 2. (*Continued*).

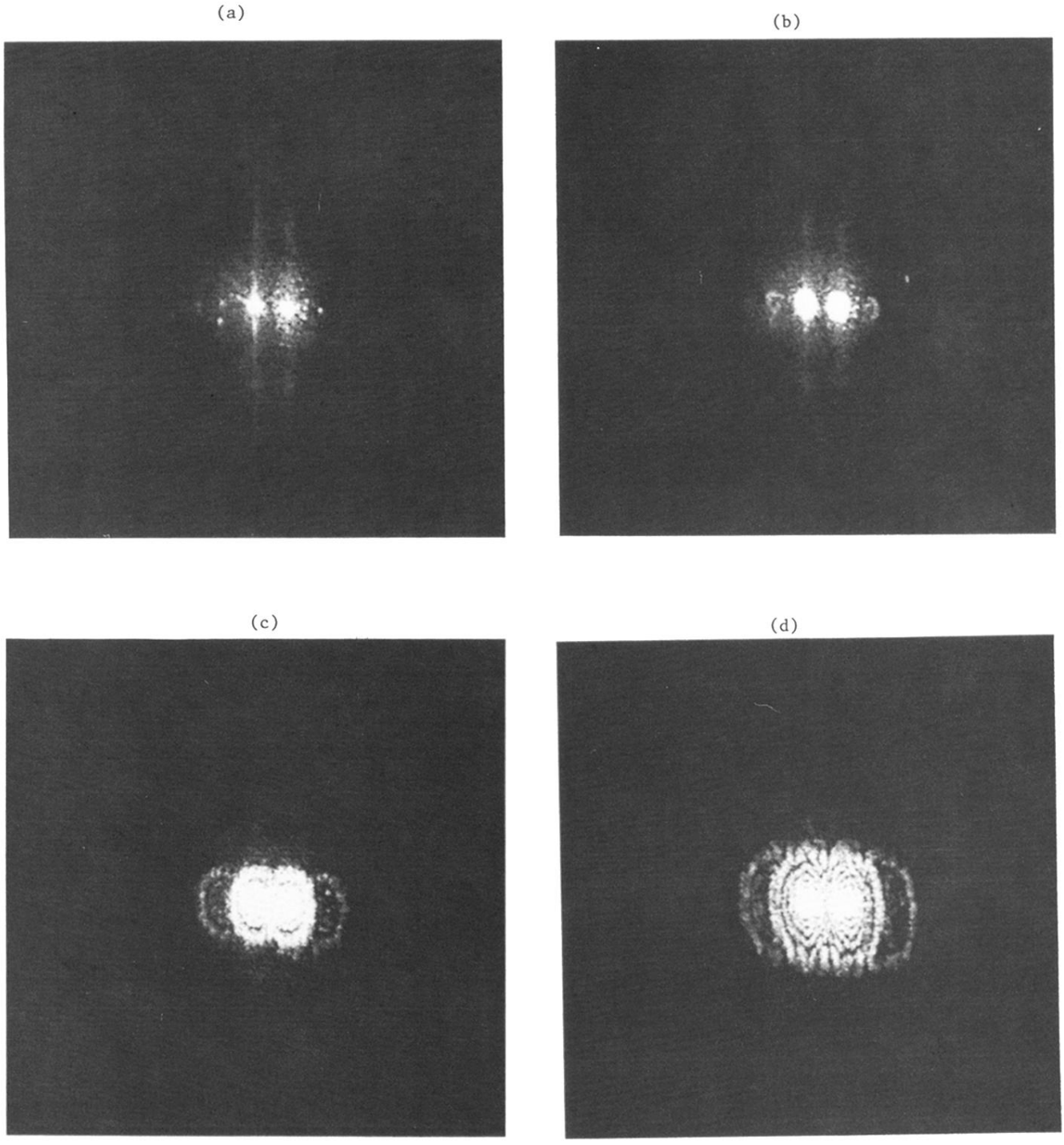

FIG. 3. Experimental results for the case theoretically modeled in Fig. 2, with images taken from a video sequence of the far-field diffraction-pattern development. The images are chosen to correspond with those shown in Fig. 2. The times are (a) 4 s; (b) 20 s; (c) 38 s; (d) 50 s; (e) 200 s.

(e)

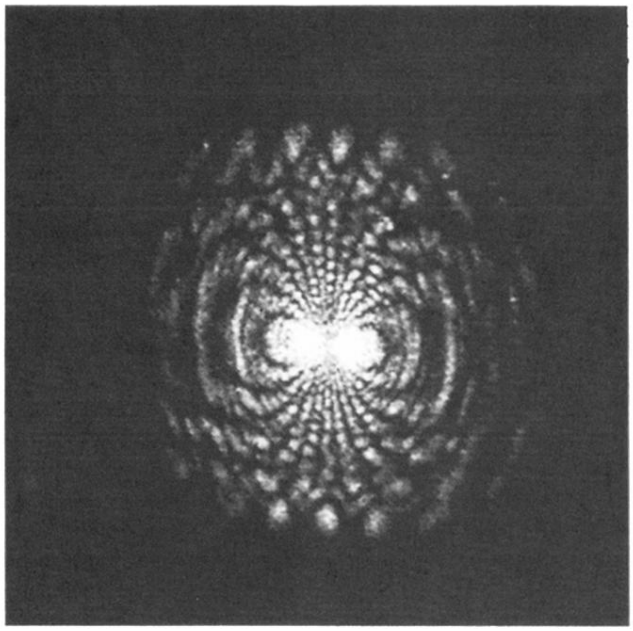

FIG. 3. (*Continued*).

(a)

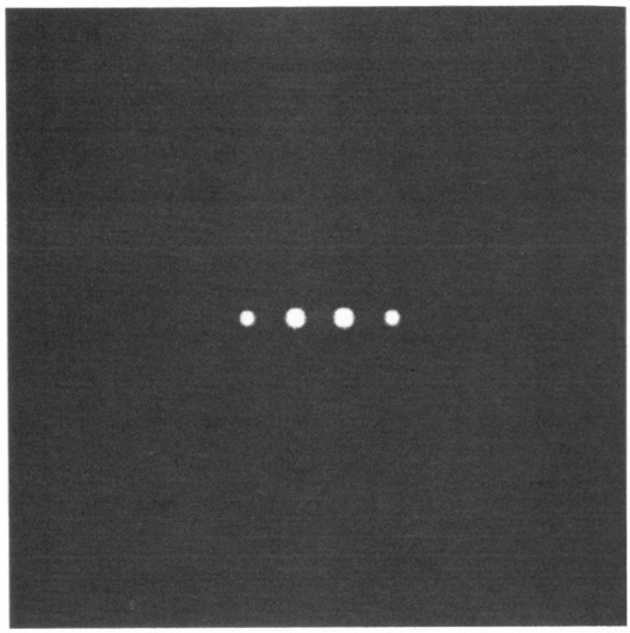

(b)

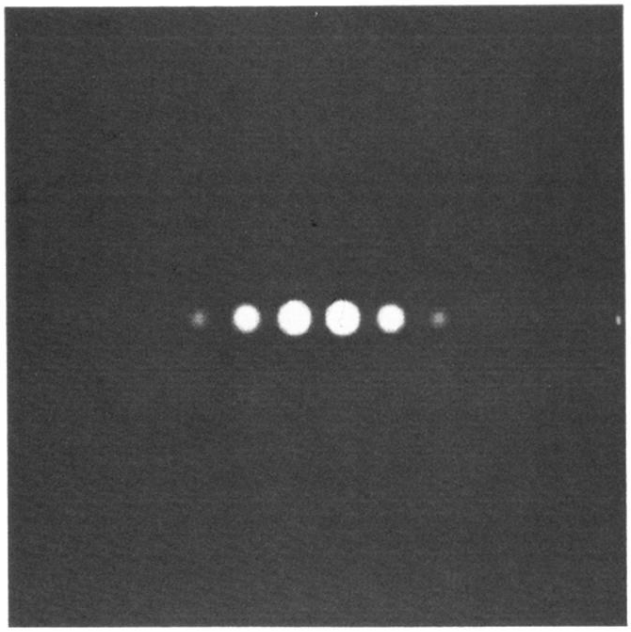

FIG. 6. Theoretical prediction of diffraction patterns for $\beta_{ext}=20°$. Only the initial development is shown for times of (a) 0.2 s and (b) 1 s, showing the prediction of up to six Raman-Nath spots in this case.

(a)

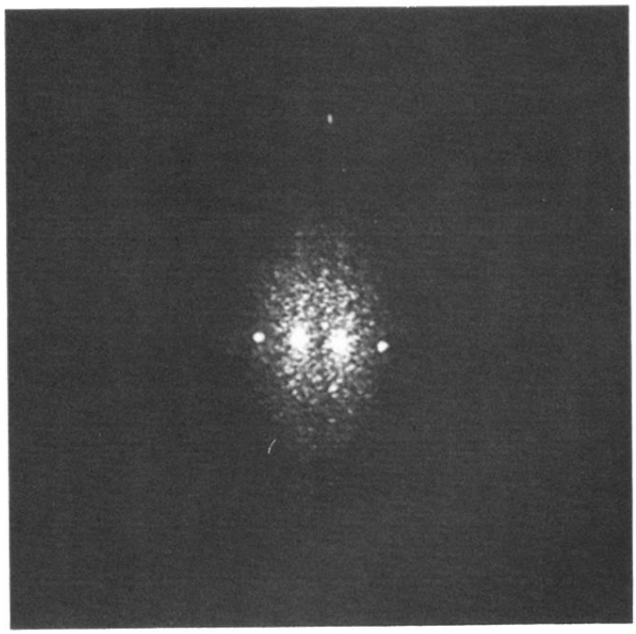

(b)

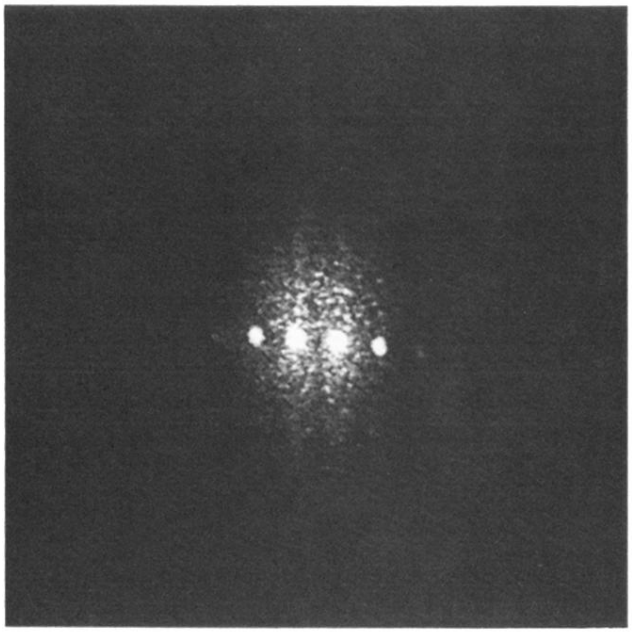

FIG. 7. Experimental results for $\beta_{ext}=20°$, corresponding to Fig. 6. the times are (a) 0.25 s and (b) 1 s, in this case in very good agreement with the theoretical predictions.

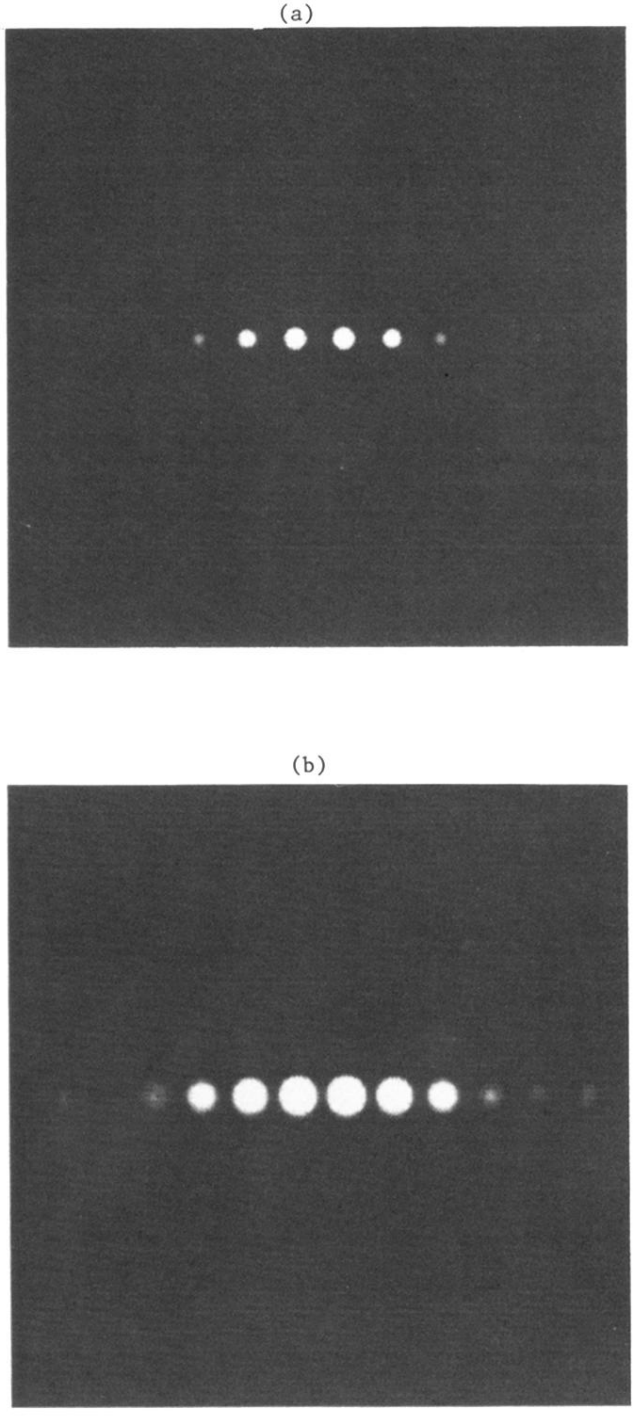

FIG. 8. Theoretical prediction for the initial development of the diffraction patterns for $\beta_{ext}=45°$. The times are (a) 0.08 s and (b) 0.4 s. In this case eight Raman-Nath spots are seen.

(a)

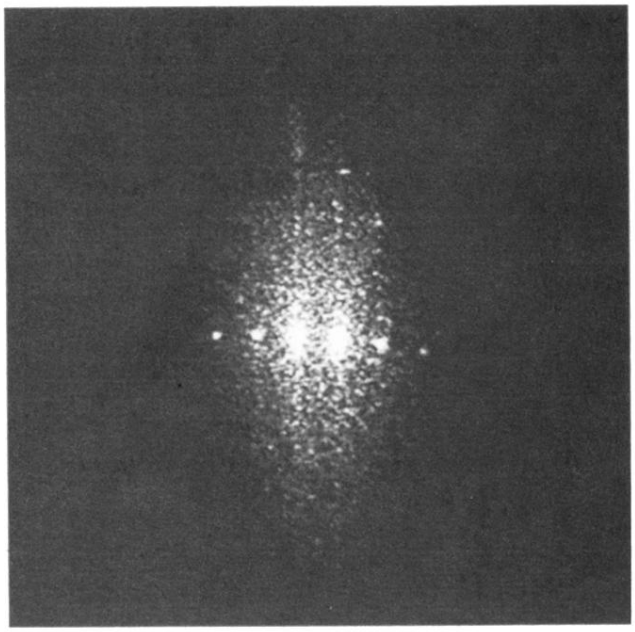

(b)

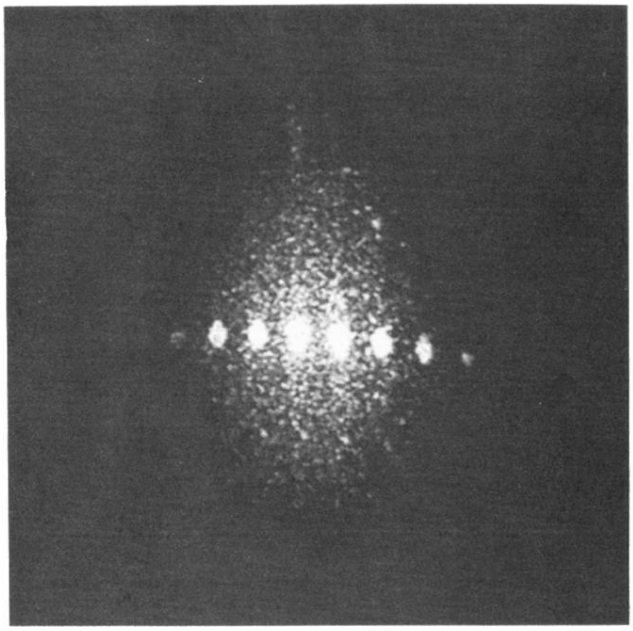

FIG. 9. Experimental results from the video for $\beta_{ext}=45°$, corresponding to the theory of Fig. 8. The times are (a) 0.12 s and (b) 0.55 s. The eight Raman-Nath spots are seen here in the experimental data as well, although there is a lot of optical scatter.